2.2
Electron Paramagnetic Resonance Spectroscopy

G. R. EATON and S. S. EATON
University of Denver, Colorado, USA

2.2.1 INTRODUCTION

Electron paramagnetic resonance (EPR) spectroscopy, also called electron spin resonance (ESR) or electron magnetic resonance (EMR) measures the absorption of microwaves by paramagnetic centers with one or more unpaired electrons.[1–5] A single unpaired electron ($S = 1/2$) can have two possible spin states, $m_s = \pm 1/2$, that are degenerate in the absence of an external magnetic field. In the presence of a magnetic field the degeneracy is lifted, and transitions can be caused to occur by supplying energy. When the energy of the microwave photons equals the separation between the spin energy levels, the system is said to be at "resonance," and there is absorption of energy by the sample. The energies for the transitions are determined by the type of paramagnetic center and are influenced by interactions with neighboring nuclei with $I > 0$ and with other unpaired electrons. The focus of this section is on samples in which the distance between paramagnetic centers is long enough that the sample can be regarded as magnetically dilute, i.e., the spectra are dominated by features of the individual centers or pairs of centers, rather than the interaction between large numbers of paramagnetic centers. In magnetically concentrated samples information can be obtained about the spin state of the metal ion, and about the strength of magnetic

interaction between the centers, but little information usually can be obtained about the g and A values that are described in the following paragraphs.

EPR spectra of magnetically dilute samples are described by a phenomenological spin Hamiltonian:

$$\hat{H} = \beta_e g \cdot B \cdot \hat{S} + \sum_i A_i \cdot \hat{I} \cdot \hat{S} \quad (1)$$

where β_e is the electron Bohr magneton, $\hat{S}$ and $\hat{I}$ are the electron and nuclear spin operators, respectively, and g and A are 3×3 matrices that define the anisotropic (orientation-dependent) interaction of the unpaired electron with the external magnetic field, B, and with nuclear spins, respectively. The g values determine the magnetic field for the center of the spectrum at a particular orientation of the molecule with respect to the magnetic field. The interaction with nuclear spins is called hyperfine interaction and causes splittings of the EPR signal. The summation in Equation (1) reflects the fact that there is a hyperfine term for each set of inequivalent nuclear spins. For some spectra it is possible to estimate g and A values by inspection, but computer simulation of the spectra usually is required to obtain precise values. When an axis system is selected in which the g and A matrices are diagonal, the elements of the g and A matrices are called the principal values. These axes are the magnetic axes for the paramagnetic center, and may not coincide with bond axes of the molecule. For metal ions with more than one unpaired electron there is an additional term in the Hamiltonian, $\hat{S} \cdot D \cdot \hat{S}$, where D is the zero-field splitting matrix, which describes the electron–electron interaction.

2.2.2 EPR PARAMETERS AND THEIR INTERPRETATION

The observation of an EPR signal can be an important test of the oxidation state of a metal ion because no signal is observed for diamagnetic metal ions. Thus, for example, there is no EPR signal for Cu^{I} or for low-spin Fe^{II}. For metals with $S = 1/2$, such as Cu^{II}, Cr^{V}, or vanadyl ion, EPR spectra can be seen at room temperature for many geometries and coordination environments. For some electron configurations (such a low-spin Fe^{III}) or geometries, relaxation times are shorter and lower temperatures are required for detection of the EPR signal. For metals with $S > 1/2$, the EPR signal is strongly dependent on the magnitude of the zero-field splitting relative to the EPR quantum, $h\nu$. For metals with $S = 3/2$ or 5/2, transitions between levels with $m_s = \pm 1/2$ can be observed even if the zero-field splitting is large, although cryogenic temperatures may be required because of faster spin lattice relaxation for these metal ions than for ones with $S = 1/2$. For metal ions with an even number of unpaired electrons and large zero-field splittings, many or all of the transition energies may be too large or too orientation dependent to observe a spectrum in powder samples, although signals may be observed for selected orientations of single crystals. As discussed in Section 2.2.3, higher microwave frequencies and magnetic fields make it possible to study spectra from metals with larger zero-field splitting than can be observed at X-band (ca. 9.5 GHz).

Spin quantitation is a key part of the EPR signal characterization.[3] EPR spectroscopy is sufficiently sensitive that signals can sometimes be observed from species that constitute only a small fraction of the potentially paramagnetic centers. For an $S = 1/2$ metal ion the double integral of the first-derivative EPR signal is proportional to the number of spins in the sample. Comparison with a spin standard can then be used to determine the spin concentration for the species of interest. Quantitation is more difficult for metal ions with $S > 1/2$ and zero-field splitting greater than the EPR quantum, because only some of the transitions may be observable for a particular microwave frequency.[6]

2.2.2.1 g Values

The g value for the free electron is 2.0023. Spin–orbit coupling results in g values for metal ions that are substantially different from the free electron value. The g values are characteristic of the electronic structure, local symmetry, and often the coordination environment. Thus, g values are powerful tools for characterization of metal complexes.[2,4,5]

2.2.2.2 A Values

The hyperfine splitting pattern in an EPR spectrum reflects the interaction of the unpaired electron with nuclear spins. The number of hyperfine lines equals $2nI+1$, where n is the number of equivalent nuclei and I is the nuclear spin. Spectra due to certain metal ions are readily recognized because of characteristic numbers of lines that arise from coupling to the metal nuclear spin: for example, vanadium (99.75% $I=7/2$), chromium (9.5% $I=3/2$, other isotopes have $I=0$), manganese (100% $I=5/2$), cobalt (100% $I=7/2$), copper (69.2% ^{63}Cu $I=3/2$ and 30.8% ^{65}Cu $I=3/2$), and molybdenum (15.9% ^{95}Mo $I=3/2$, 9.6% ^{97}Mo $I=3/2$, other isotopes have $I=0$). The magnitude of the hyperfine coupling to the metal nuclear spin is proportional to the electron spin density on the metal.

Hyperfine splitting due to interaction with ligand nuclei with $I>0$ reflects the extent of spin delocalization onto neighboring atoms and can be used to characterize the types and numbers of such nuclei. In cases where these couplings are too small to be resolved in the EPR spectra, electron nuclear double resonance (ENDOR) or electron spin echo envelope modulation (ESEEM) can be used to measure the couplings as discussed in Chapter 2.3. Modern calculational tools are approaching the capabilities required to calculate g and A values from electronic wave functions.[7,8] However, much of the spectroscopy that has been performed to date has used empirical correlations to interpret g and A values.

2.2.2.3 Temperature Dependence

For some metal ions, such as high-spin Co^{II} ($S=3/2$)[9] or iron–sulfur clusters,[10] the electron spin relaxation time is strongly temperature dependent. If the relaxation time becomes too short, then the signal becomes so broad that the signal is essentially undetectable. For many high-spin Co^{II} complexes and iron–sulfur clusters, detection of an EPR signal requires temperatures in the liquid helium range.

For spin-coupled systems the EPR spectrum may be temperature dependent due to temperature-dependent populations of excited states. For example, in strongly antiferromagnetically coupled copper(II) dimers, there is no EPR signal at low temperatures, but a characteristic triplet ($S=1$) signal grows in as the temperature is increased due to thermal population of the excited state.[11]

Dynamic processes that interconvert conformations of a metal complex can be detected by EPR if the rate of the process is comparable to separations between peaks in the EPR spectrum.[12] For splittings on the order of a few milliteslas (tens of MHz) that timescale corresponds to rates on the order of 10^7 to $10^8\,s^{-1}$, which is significantly faster than the NMR timescale.

2.2.2.4 Electron Spin Relaxation Times

Electron spin relaxation times reflect both intramolecular and intermolecular dynamic processes. In favorable cases relaxation times can be estimated from progressive power-saturation measurements, but more accurate values can be obtained by pulsed time domain techniques.[13] For metal ions with low-lying excited states the temperature dependence of relaxation times can be used to determine the energy of the excited state.[9]

2.2.2.5 Phase of Sample

EPR spectra can be observed in gas, liquid, or solid phases. Interpretation of gas-phase EPR spectra is complicated by coupling between the spin angular momentum and rotational angular momentum and has not been used for transition metal complexes. For small metal complexes in fluid solution, the rate of tumbling typically is fast enough to largely average the g and A anisotropy, and the spectra are described by the isotropic averages of the g and A values: $g_{iso}=(g_x+g_y+g_z)/3$ and $A_{iso}=(A_x+A_y+A_z)/3$. For metal ions with significant g and/or A anisotropy, line shapes in fluid solution often are strongly dependent on the rate of tumbling. When a metal complex is immobilized, either by freezing a solution or by doping into a diamagnetic host, the resulting sample contains a random distribution of orientations of the metal ion with respect to the external magnetic field. Analysis of the spectra usually can provide the three principal components of the g matrix and the principal components of resolved

hyperfine splittings. To fully characterize g and A matrices and the orientations of the principal axes of the matrices with respect to the molecular axes requires spectra from a doped single crystal as a function of orientation of the crystal with respect to the magnetic field.[1]

2.2.3 SELECTION OF MICROWAVE FREQUENCY

Historically, the vast majority of EPR experiments have been performed at a microwave frequency between about 9 and 9.5 GHz, which falls in the range that is called X-band. At this microwave frequency the free electron g value corresponds to a resonant field of about 3,300 G (330 mT). Relatively recently, commercially available spectrometers have become available over a widening range of frequencies: currently about 1 GHz (L-band) to 95 GHz (W-band). It now becomes important to consider what EPR frequency is optimum to answer a particular question. For some questions, the clearest answers are obtained by comparing spectra as a function of microwave frequency.[14]

As the magnetic field is increased, the separation of features in the spectra that arise from g value differences becomes larger.[15] For example, the 10-fold increase in microwave frequency from 9.5 to 95 GHz results in a 10-fold increase in separations of features in the spectra that arise from g anisotropy. Resolution of these features may be key to determining whether the effective symmetry at a metal site is axial or rhombic. When the zero-field splitting for metal ions with $S > 1/2$ is greater than the EPR quantum ($h\nu$) the energies for some transitions may be too large to detect. By increasing the microwave frequency, higher energy transitions become accessible, so higher microwave frequencies and the corresponding high magnetic field strengths are particularly useful for metal ions with $S > 1/2$ and large zero-field splittings.[16] Higher magnetic fields also sometimes make it possible to obtain EPR signals for complexes with an even number of unpaired electrons such as Ni^{II} ($S = 1$)[17] and Mn^{III} ($S = 2$).[18]

However, for other problems, microwave frequencies lower than 9.5 GHz can be advantageous. At lower microwave frequencies the relative importance of g anisotropy is decreased relative to hyperfine interaction. A particularly dramatic example is the improved resolution of nitrogen hyperfine structure in Cu^{II} complexes that can be achieved with spectra at about 2 GHz (S-band).[19]

2.2.4 CONTINUOUS WAVE VS. PULSED EXPERIMENTS

The EPR spectra for most transition metal complexes in rigid lattices extend over hundreds to thousands of gauss. With current pulsed microwave technology it is only possible to excite bandwidths of about 50 gauss, so Fourier transform EPR is limited to relatively narrow spectra. Most pulsed EPR experiments examine only a limited segment of a spectrum. This permits sequential examination of sets of spins for which there is a small distribution of orientations of the magnetic axes with respect to the external magnetic field, which is called orientation selection (see Chapter 2.3, Section 2.3.4). Pulsed experiments also require relaxation times longer than about 0.1 μs, which means that for most metal ions experiments must be performed at cryogenic temperatures. Within these limitations, there is a wide range of pulsed experiments that have been designed to obtain specific information about relaxation times (Section 2.2.5.5) and nuclear hyperfine interactions (Chapter 2.3).[20]

2.2.5 SPECTRA OF $Cu(DTC)_2$

The preceding generalizations concerning information content from various types of EPR experiments can be made more concrete by considering the series of spectra for $Cu(dtc)_2$ shown in Figures 1–5. The spectra for this complex are better resolved than for most transition metal complexes, which makes them well suited to be a tutorial example.

2.2.5.1 Single Crystal

$Ni(dtc)_2$ is square–planar and diamagnetic which makes it a convenient host for examining square–planar $Cu(dtc)_2$. The CW spectrum for one orientation of a single crystal of $Ni(dtc)_2$

doped with $Cu(dtc)_2$ is shown in Figure 1. Continuous wave EPR spectra routinely are detected by magnetic field modulation with phase-sensitive detection which gives the first derivative of the microwave absorption as shown in Figure 1a. The corresponding absorption spectrum, obtained by integration of the spectrum in Figure 1a is shown in Figure 1b. In the single-crystal spectrum there are distinct peaks in the absorption spectrum with negligible intensity between the peaks. There are two inequivalent sites of substitution in this oriented crystal, so there are two distinct orientations of the magnetic axes of the Cu^{II} center with respect to the external magnetic field (Figure 1). The ratio of populations of the two copper isotopes (^{63}Cu and ^{65}Cu) at natural abundance is approximately 2:1. Due to difference in the magnetogyric ratios for the two isotopes, the hyperfine coupling to ^{65}Cu is 1.07 times larger than for ^{63}Cu so there are separate lines for the two isotopes as marked for the low-field lines of site 1. For each isotope, at each site, the spectrum is split into four lines because of hyperfine coupling to the copper nuclear spin ($I = 3/2$), which can have $m_I = -3/2$, $-1/2$, $1/2$, or $3/2$. Thus, there is a total of 16 lines in the single-crystal spectrum, all of which are resolved in the first derivative display. The decreased resolution in the absorption spectrum compared to that of the first derivative is one of the main reasons why EPR spectra are usually displayed as first derivatives.

The spacing between adjacent hyperfine lines (Figure 1) is approximately equal to the copper hyperfine coupling for that orientation of the molecule in the magnetic field. The discrepancy between the true value of A and the value estimated by measuring the splitting is due to terms that arise from solving the Hamiltonian (Equation (1)).[1] In a second-order perturbation analysis these terms are proportional to m_I^2 times A^2/B_{res} where A is the hyperfine coupling constant and B_{res} is the resonant field.[1,4,5] These terms, which commonly are called "second order corrections," become more significant as A increases and B_{res} decreases, so they are of particular concern for large metal hyperfine couplings. For each Cu isotope at each of the sites, the copper hyperfine

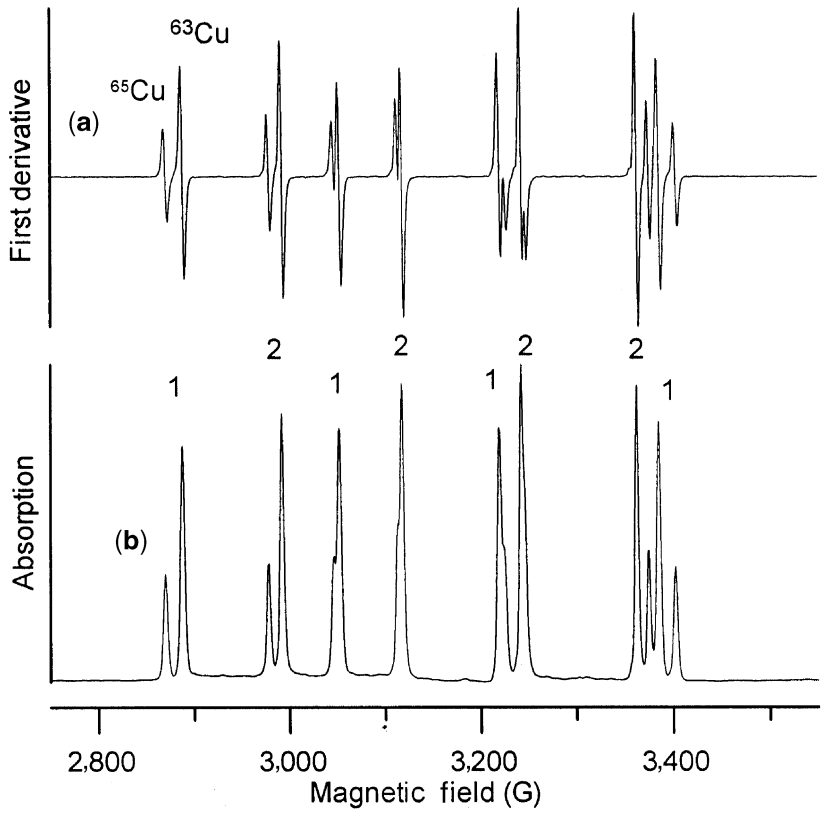

Figure 1 X-band (9.119 GHz) CW spectrum of a single crystal of $Ni(dtc)_2$ doped 1:500 with $Cu(dtc)_2$ obtained at 100 K with 0.04 mW microwave power and 1.0 G modulation amplitude displayed as the traditional first derivative (a). Computer integration of the spectrum in A gave the absorption spectrum (b). The lines for the two inequivalent sites in the crystal are marked with the numbers "1" and "2." The four hyperfine lines for each isotope at each site are due to copper nuclear spin states with $m_I = -3/2$, $-1/2$, $1/2$, and $3/2$. Computer simulations showed that the angle between the external magnetic field and the magnetic z-axis is 20° for site 1 and 49° for site 2.

interaction can be estimated by measuring the spacing between the corresponding lowest-field line and the highest-field line (the $m_I = \pm 3/2$ lines) and dividing by three. This measurement is more precise than the spacing between adjacent hyperfine lines because the second order corrections contribute equally to the low-field and high-field lines. The g value can be estimated from the field that is half-way between the two middle hyperfine lines ($m_I = \pm 1/2$ lines), using the expression $g = h\nu/\beta B$. The use of the two $m_I = \pm 1/2$ lines is better for the calculation of the g value than the $m_I = \pm 3/2$ lines because the second order corrections are smaller for the $m_I = \pm 1/2$ lines. It must be stressed, however, that parameters estimated from the spectra in this fashion are not accurate and to obtain accurate values it is important to use computer simulations that are based on diagonalization of the Hamilton matrix or a perturbation calculation to at least second order. The orientation of the crystal for which spectra are shown in Figure 1a resulted in an angle of 20° between the external magnetic field and the z-axis for site 1 and an angle of 49° for site 2. As is characteristic of square-planar Cu^{II},[21] the g and A values are larger along the z-axis (perpendicular to the molecular plane) and smaller in the x,y plane. Since $h\nu = g\beta B$, a decrease in g value results in resonance at higher magnetic field (B) so the center of the spectrum is at higher field for site 2 than for site 1.

2.2.5.2 Powder Spectra

The term "powder" EPR spectrum implies that there is a random distribution of orientations of the molecules with respect to the external magnetic field. This random distribution can be achieved by rapidly cooling a solution to form a glass or with a large number of tiny crystallites. The X-band (9.107 GHz) spectrum of a powdered sample of $Ni(dtc)_2$ doped with $Cu(dtc)_2$ is shown as the first-derivative and absorption displays in Figures 2a and 2b, respectively. The dominant features of the first-derivative spectrum occur at magnetic fields where there is an abrupt change in the absorption spectrum. These positions correspond to extrema in the orientation dependence of the transitions, although the terminology peak or line is commonly used in describing the spectra. The four extrema marked as "z" in Figure 2a correspond to the four copper hyperfine lines for molecules aligned with the magnetic field along the magnetic z-axis. For the low-field and high-field extrema, the ^{63}Cu and ^{65}Cu contributions are resolved. The four extrema marked as "$\perp$" correspond to the four copper hyperfine lines for molecules oriented with the magnetic field in the molecular plane. At X-band the g values for $Cu(dtc)_2$ along the x and y axes are so similar that the spectrum appears to be axial. It is important to remember that for each hyperfine line (each value of m_I), the spectrum actually extends from the parallel (z-axis) to the perpendicular extrema. Intermediate orientations of the molecule are at resonance at magnetic fields intermediate between the corresponding extrema, but the absorption spectrum changes relatively slowly with magnetic field in these intermediate regions, so the slope is small, and the first derivative signal is close to baseline. This orientation dependence is more clearly seen in the absorption display (Figure 2b) than in the first derivative display of the spectrum. The spectrum of $Cu(dtc)_2$ in glassy toluene solution at 100 K is very similar to that shown for the doped solid in Figure 2, because it, too, represents a random distribution of molecular orientations, and the g and A values in toluene solution are similar to those in the doped solid.

The W-band (ca. 95 GHz) spectrum of $Ni(dtc)_2$ doped with $Cu(dtc)_2$ is shown in Figure 3. To achieve resonance at the higher microwave frequency requires a correspondingly higher magnetic field, which at 95 GHz requires a superconducting magnet. The hyperfine interaction is independent of field, but the separation between extrema due to inequivalent g values increases proportional to magnetic field. Thus, at W-band the separation between g_z and g_x or g_y is much larger than the hyperfine splitting for either extrema. In addition, at W-band, the perpendicular region of the spectrum is resolved into two sets of four extrema due to observable inequivalence between g_x and g_y.

2.2.5.3 Line Widths

For $Cu(dtc)_2$ the line widths of the peaks in the single-crystal spectra and of the extrema in the powder spectra are a few gauss. These line widths are unusually small for a metal complex in a solid sample, which is due to a combination of several factors. (i) Unresolved nuclear hyperfine splitting can be a major contributor to line widths for many complexes. However, for $Cu(dtc)_2$ the directly coordinated ligand atoms are sulfur, for which only 0.75% has a nuclear spin. The nearest nuclei with a high abundance of nuclear spin are the nitrogens that are three bonds removed from

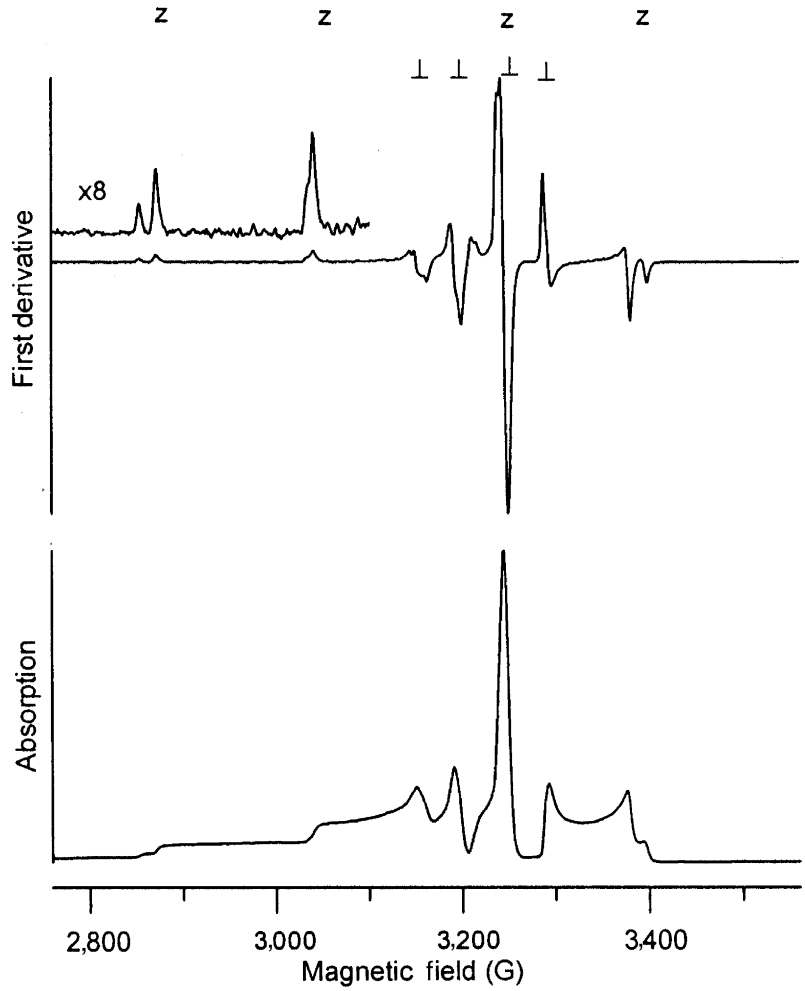

Figure 2 X-band (9.107 GHz) CW spectrum of a powdered sample of $Ni(dtc)_2$ doped 1:500 with $Cu(dtc)_2$ obtained at 150 K with 1.0 mW microwave power and 1.0 G modulation amplitude and displayed as the traditional first derivative (a). Computer integration of the spectrum in *A* gives the absorption spectrum (b). The turning points in the powder pattern that correspond to the four copper hyperfine lines for molecules aligned with the magnetic field along the magnetic *z*-axis or in the perpendicular plane are marked as "z" or "⊥", respectively.

the Cu. The couplings to these nuclei are so small that measurement of the hyperfine interaction requires either ENDOR or ESEEM as described in Chapter 2.3. (ii) As discussed earlier, the electron spin relaxation times for square–planar Cu^{II} in this ligand environment are long enough that relaxation does not make a significant contribution to the line widths at the temperatures for which the spectra in Figures 1–3 were obtained. (iii) If the molecule is relatively flexible or the host environment forces a range of distortions, there can be a distribution of values for the principal components of the g and A matrices, which is known as "*g* strain" and "*A* strain," and results in broadening of the lines in the spectra.[22,23] For $Cu(dtc)_2$ in glassy toluene solution or doped into $Ni(dtc)_2$ the geometry is relatively well defined so *g* and *A* strain are relatively small.

2.2.5.4 Fluid Solution

The X-band CW spectrum of $Cu(dtc)_2$ in toluene solution (Figure 4) consists of four lines with a splitting of $A_{iso} = 78$ G. The tumbling of the molecule is fast enough to largely average the anisotropy of the *g* and *A* matrices. The lines are narrow enough that the contributions from the ^{63}Cu and ^{65}Cu isotopes are resolved on the high-field line and partially resolved on the low-field

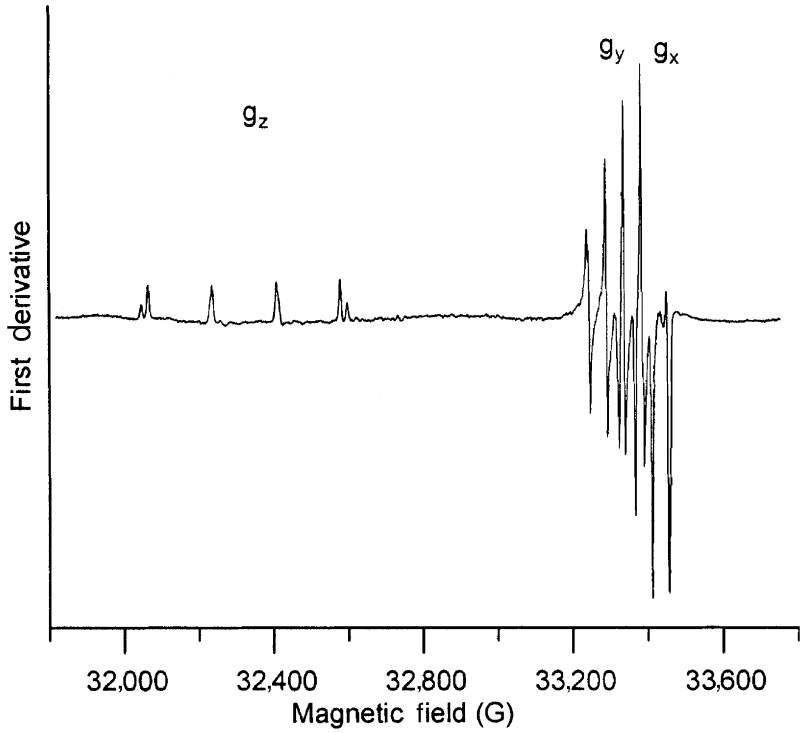

Figure 3 W-band (94.19 GHz) CW spectrum of a powdered sample of $Ni(dtc)_2$ doped 1:500 with $Cu(dtc)_2$ obtained at 50 K with 60 nW of microwave power and 4 G modulation amplitude, and displayed as the first derivative of the microwave absorption. The turning points in the powder pattern that correspond to g_z, g_y, and g_x are marked. Copper hyperfine coupling is resolved along each of the principal axes. Spectrum was obtained by Dr. Ralph Weber, Bruker Instruments.

line. The amplitudes of the four lines are different because of differences in the line widths. These line width differences can be analyzed to determine the tumbling correlation time,[24,25] which depends upon microscopic viscosity, and can be very different from macroscopic viscosity due to specific interactions between solute and solvent. For $Cu(dtc)_2$ in toluene at room temperature the tumbling correlation time is about 4×10^{-11} sec/rad.[26]

2.2.5.5 Electron Spin Relaxation Times

Although power saturation curves can be used as a monitor of changes in relaxation times, for most samples pulsed measurements are required to accurately define the relaxation times and to characterize contributions from other competing processes that take spins off resonance.[13] Long-pulse CW saturation recovery measurements for $Cu(dtc)_2$ doped into $Ni(dtc)_2$ found that T_{1e} decreased from 180 μs at 26 K to 0.6 μs at 298 K, and the temperature dependence could be modeled with a Raman process and a local vibrational mode.[27] The relaxation times for $Cu(dtc)_2$ between 30 and 160 K were very similar for the doped $Ni(dtc)_2$ solid and for glassy toluene solution, which showed that the surrounding environment had little impact on the relaxation. However, the relaxation times for $Cu(dtc)_2$ are much longer than for a less rigid Cu^{II} complex, which highlights the important role of molecular rigidity in relaxation processes in the solid state.[28]

A two-pulse spin echo experiment consists of a 90°-τ-180°-τ-echo pulse sequence (see Chapter 2.3, Section 2.3.2). The amplitude of the echo is monitored as a function of the time τ between the echoes, and the decay time constant is denoted as T_m, the phase memory decay time.[20] T_m is strongly dependent upon dynamic processes that result in echo dephasing on the time scale of the experiment. In $Cu(dtc)_2$ the coupling of the unpaired electron to the spins of the protons of the ethyl groups is too small to be resolved in the CW spectra. However, when the rate of rotation of the

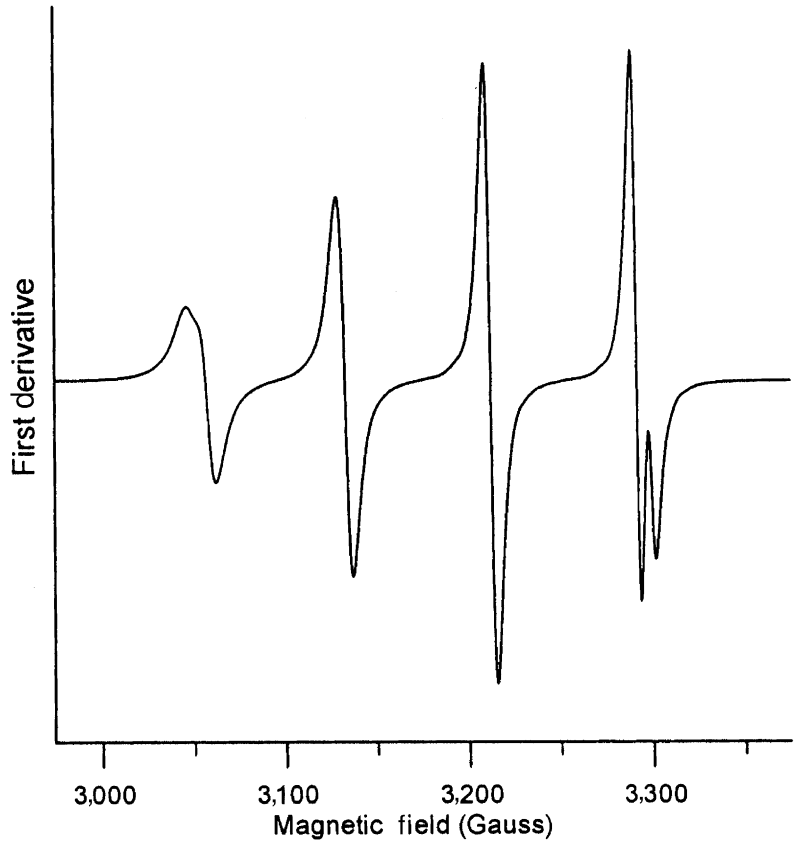

Figure 4 X-band (9.099 GHz) CW spectrum of 1.0 mM $Cu(dtc)_2$ in toluene solution at 294 K obtained with 50 mW microwave power and 0.5 G modulation amplitude, and displayed as the first derivative of the microwave absorption.

methyl groups is comparable to the inequivalence between couplings to individual methyl protons, the rotation results in substantial decreases in T_m. The temperature dependence of T_m has been analyzed to determine the barrier to methyl group rotation in $Cu(dtc)_2$ and in Cr^V complexes of ligands that contain methyl groups.[29,30]

Figure 5 shows the field-swept echo-detected spectrum of $Cu(dtc)_2$ in glassy toluene solution at 30 K. The spectrum was recorded by setting the τ value for the two-pulse spin echo sequence to 1 μs and recording the echo amplitude as a function of magnetic field. If T_m were uniform through the spectrum, the echo-detected spectrum (Figure 5) should match the absorption spectrum (Figure 2b). However, there are substantial differences that are particularly conspicuous in the regions highlighted by the vertical arrows. In the absorption spectrum the signal amplitude increases abruptly near the low-field extrema for the $m_I = -3/2$ ^{65}Cu and ^{63}Cu lines at about 2,850 G then slowly increases between about 2,900 and 3,000 G. Another abrupt increase in signal intensity occurs at the low-field extrema for the parallel orientation of the $m_I = -1/2$ transition at about 3,040 G. By contrast, in the echo-detected spectrum the amplitude of the spectrum is much lower between 2,900 and 3,000 G than at 2,850 G. This dramatic difference between the CW absorption spectrum and the echo-detected spectrum occurs because T_m is much shorter between 2,900 G and 3,000 G than near the extrema. This behavior arises from low-amplitude vibrations (librations) on the timescale of the spin echo experiment that move spins off resonance. The effects of librations on T_m are particularly evident in this region of the spectrum because the transition energy is so orientation dependent that reorientation by a few degrees is sufficient to move spins that were excited by the first pulse out of the range of detection for the second pulse.[31] In the doped solid sample at the same temperature (30 K), variation of T_m through the spectrum is much less than for the glassy solution, which highlights the lower mobility of the $Cu(dtc)_2$ in the doped solid than in glassy solution.

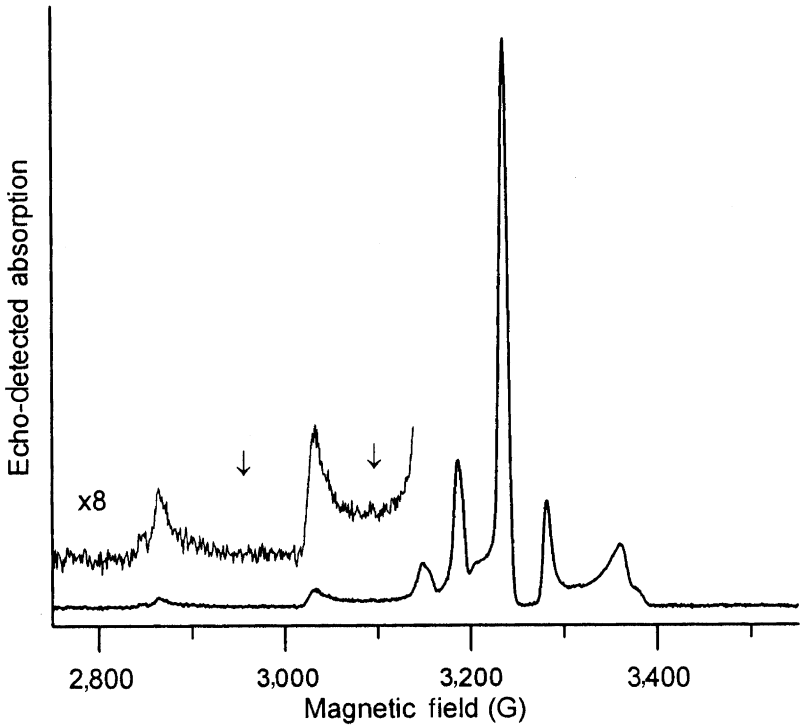

Figure 5 X-band (9.101 GHz) two-pulse spin-echo detected absorption spectrum of 2.0 mM $Cu(dtc)_2$ in glassy toluene solution at 30 K, obtained with 20 and 40 ns pulses and a fixed time between the pulses of 1 μs.

2.2.6 BIOINORGANIC EXAMPLES

Many examples of applications of EPR can be found in the discussions of individual classes of compounds in this compendium. Here we present a few examples of types of problems to which EPR has been recently applied, with an emphasis on the strategies that were used to obtain electronic and structural information.

2.2.6.1 Blue Copper Model Complexes for Cu^{II}-thiolate Complexes and Fungal Laccase

The EPR spectrum of a 3-coordinate [2N + S] model complex exhibited nitrogen hyperfine splitting of about 30 MHz in the perpendicular region of the spectrum, which was not observed in fungal laccase.[7] Analysis of the isotropic and anisotropic components of the nitrogen hyperfine interaction showed that the HOMO of the complex had ~25% nitrogen covalency. The EPR results, together with S and Cu XAS experiments, made it possible to account for essentially all of the covalency in the HOMO of the model complex. The nitrogen covalency is substantially smaller for the blue copper centers in fungal laccase or plastocyanin than for the model complex. The covalency of the Cu center in the model complex could be reproduced by DFT calculations.[7]

2.2.6.2 Dinuclear Cu_A Site in Cytochrome C Oxidase and Nitrous Oxide Reductase

EPR spectra at multiple microwave frequencies permitted identification of the Cu_A site in these proteins as dinuclear well before this geometry was characterized crystallographically.[32,33] The comparison of spectra at several frequencies (L-band (1.2 GHz), S-band (4 GHz), C-band (6 GHz), X-band (9 GHz), and Q-band (35 GHz)) coupled with computer simulations was key to the characterization because different portions of the spectra are better resolved at different

microwave frequencies. A distinctive feature of the EPR spectra of this center is the small copper hyperfine splitting (38 G) on the g-parallel lines. Also, comparison of the spectra at multiple microwave frequencies provided convincing evidence that the hyperfine splitting pattern was seven lines, not four lines. Based on spectra at a single microwave frequency it would be very difficult to unambiguously eliminate the possibility that the seven lines arose from overlapping hyperfine splittings along inequivalent hyperfine axes. Isotopically enriched ^{63}Cu or ^{65}Cu was used to decrease the complexity of the spectra and to improve the resolution of the copper hyperfine splitting. In addition, the increase in the hyperfine coupling by a factor of 1.07 between ^{63}Cu and ^{65}Cu for nitrous oxide reductase demonstrated that the hyperfine splitting was due to copper and not some other nucleus. The data all point to a binuclear center with one unpaired electron delocalized over two copper nuclei, i.e., a formal oxidation state of 1.5 for each copper atom. The electron spin relaxation times for the Cu_A signal are substantially shorter than for type I or type II monomeric copper, which also pointed to a dinuclear center.

2.2.6.3 Oxygen-evolving Complex in Photosystem II

The manganese cluster in the oxygen-evolving complex of Photosystem II presents a challenge for EPR because of the complexity of the spin system. The Mn $I = 5/2$ results in six hyperfine lines. Additional splittings result from electron spin $S > 1/2$, which is further complicated by electron spin–spin coupling within the cluster. Despite the name "multiline" signal, the spectra of the manganese cluster at X-band are deceptively simple, and there are many more transitions than give resolved lines.[34,35] Spectra at multiple frequencies and careful computer simulations with attention to relative intensities of features have been crucial to showing that there is a cluster of four Mn atoms. Even so, the parameters obtained by simulations for the Mn centers are not unique. For these membrane-bound proteins an additional useful tool is one-dimensional ordering of the molecules on a mylar film. Orientation of the mylar film in the EPR resonator and subsequent rotation of the film provides orientation-dependent spectra that provide key insights. This technique has been used to determine the distance between the manganese cluster and the neighboring tyrosyl radical, and the orientation of the interspin vector relative to the plane of the membrane.[36] EPR has been extensively used to define distances between other pairs of paramagnetic centers in photosynthetic systems.[37]

2.2.7 SUMMARY

EPR encompasses a wide range of powerful methods to probe the geometry and electronic structure of paramagnetic metal complexes. Techniques that were until recently available only in a few specialized laboratories are becoming more widely available in commercial spectrometers. The challenge to the experimentalist is to select the set of experiments that will most directly address the particular question of interest.

2.2.8 REFERENCES

1. Weil, J. A.; Bolton, J. R.; Wertz, J. E. *Electron Paramagnetic Resonance: Elementary Theory and Practical Applications* Wiley-Interscience: New York, 1994.
2. Pilbrow, J. R. *Transition Ion Electron Paramagnetic Resonance* 1990, Oxford University Press, New York.
3. Eaton, S. S.; Eaton, G. R. Electron Paramagnetic Resonance. In *Analytical Instrumentation Handbook*, 2nd Ed.; Ewing, G. W., Ed.; Dekker: New York, 1997, pp 767–862.
4. Kuska, H. A.; Rogers, M. T. Electron Spin Resonance of Transition Metal Complex Ions. In *Coordination Chemistry*, ACS Symposium Series. No. 168, Martell, A. E., Ed. Van Nostrand: New York, 1971, 186–263.
5. McGarvey, B. R. *Trans. Met. Chem. Ser. Adv.* **1966**, *3*, 89–201.
6. Silverstone, H. J.; Gaffney, B. J. *Biol. Magn. Reson.* **1993**, *13*, 1–57.
7. Randall, D. W.; George, S. D.; Holland, P. L.; Hedman, B.; Hodgson, K. O.; Tolman, W. B.; Solomon, E. I. *J. Am. Chem. Soc.* **2000**, *122*, 11632–11648.
8. Larsen, S. C. *J. Phys. Chem.* **2001**, *105*, 8333–8338.
9. Makinen, M. W.; Wells, G. B. *Metal Ions in Biological Systems* **1987**, *22*, 129–206.
10. Beinert, H.; Sands, R. H. Biological Applications of EPR Involving Iron. In *Foundations of Modern EPR*, Eaton, G. R.; Eaton, S. S.; Salikov, K. M. Eds., World Scientific: Singapore, 1998, pp 379–409.
11. Wasson, J. R.; Shyr, C.-I.; Trapp, C. *Inorg. Chem.* **1968**, *7*, 469–475.
12. Folgado, J. V.; Henke, W.; Allman, R.; Stratemeier, H.; Beltran-Porter, D.; Rojo, T.; Reinen, D. *Inorg. Chem.* **1990**, *29*, 2035–2042.

13. Eaton, S. S.; Eaton, G. R. *Biol. Magn. Reson.* **2000**, *19*, 29–154.
14. Basosi, R.; Antholine, W. E.; Hyde, J. S. *Biol. Magn. Reson.* **1993**, *13*, 103–150.
15. Eaton, S. S.; Eaton, G. R. EPR at High Magnetic Fields and High Frequencies. In *Handbook of Electron Spin Resonance*, Poole, C. P. Jr.; Farach, H. A., Eds, AIP Press, 1999, Vol. 2, pp 345–370.
16. Wood, R. M.; Stucker, D. M.; Jones, L. M.; Lynch, W. B.; Misra, S. K.; Freed, J. H. *Inorg. Chem.* **1999**, *38*, 5384–5388.
17. van Dam, P. J.; Klaasen, A. A. K.; Reijerse, E. J.; Hagen, W. R. *J. Magn. Reson.* **1998**, *130*, 140–144.
18. Barra, A.-L.; Gatteschi, D.; Sessoli, R.; Abbati, G. L.; Cornia, A.; Fabretti, A. C.; Uytterhoeven, M. G. *Angew. Chem. Int. Ed. Engl.* **1997**, *36*, 3239–2331.
19. Hyde, J. S.; Froncisz, W. *Ann. Rev. Biophys. Bioeng.* **1982**, *11*, 391–417.
20. Schweiger, A.; Jeschke, G. *Principles of Pulse Electron Paramagnetic Resonance* 2001, Oxford University Press, Oxford, UK.
21. Hathaway, B. J.; Billing, D. E. *Coord. Chem. Rev.* **1970**, *5*, 143–207.
22. Froncisz, W.; Hyde, J. S. *J. Chem. Phys.* **1980**, *73*, 3123–3131.
23. Hagen, W. R. g-Strain: Inhomogeneous Broadening in Metalloprotein EPR. In *Advanced EPR: Applications in Biology and Biochemistry*, Hoff, A. J., Ed., Elsevier: Amsterdam, 1989, Chapter 2.
24. Wilson, R.; Kivelson, D. *J. Chem. Phys.* **1966**, *44*, 154–161.
25. Chasteen, N. D.; Hanna, M. W. *J. Phys. Chem.* **1972**, *76*, 3951–3956.
26. Heinig, M. J.; Ph.D. Thesis, University of Denver, 1979.
27. Zhou, Y.; Bowler, B.; Eaton, S. S.; Eaton, G. R. *J. Magn. Reson.* **1999**, *139*, 165–174.
28. Du, J.-L.; Eaton, G. R.; Eaton, S. S. *J. Magn. Reson. A* **1995**, *117*, 67–72.
29. Nakagawa, K.; Candelaria, M. B.; Chik, W. W. C.; Eaton, S. S.; Eaton, G. R. *J. Magn. Reson.* **1992**, *98*, 81–91.
30. Du, J.-L.; Eaton, G. R.; Eaton, S. S. *Appl. Magn. Reson.* **1994**, *6*, 373–8.
31. Du, J.-L.; More, K. M.; Eaton, S. S.; Eaton, G. R. *Israel J. Chem.* **1992**, *32*, 351–355.
32. Antholine, W. E.; Kastrau, D. H. W.; Steffens, C. M.; Buse, G.; Zumft, W. G.; Kroneck, P. M. H. *Eur. J. Biochem.* **1992**, *209*, 875–881.
33. Antholine, W. E. *Adv. Biophys. Chem.* **1997**, *6*, 217–246.
34. Zheng, M.; Dismukes, G. C. *Inorg. Chem.* **1996**, *35*, 3307–3319.
35. Lakshmi, K. V.; Eaton, S. S.; Eaton, G. R.; Frank, H. A.; Brudvig, G. W. *J. Phys. Chem. B* **1998**, *102*, 8327–8335.
36. Lakshmi, K. V.; Eaton, S. S.; Eaton, G. R.; Brudvig, G. W. *Biochemistry* **1999**, *38*, 12758–12767.
37. Lakshmi, K. V.; Brudvig, G. W. *Biol. Magn. Reson.* **2001**, *19*, 513–567.

Comprehensive Coordination Chemistry II
ISBN (set): 0-08-0437486

Volume 2, (ISBN 0-08-0443249); pp 37–48